



Investigation on the development and building of a voice coil actuator-driven XY micro-motion stage with dual-range capabilities

Prasanna P. Raut¹ · A. S. Rao¹ · Shrishail Sollapur² · Devakant D. Baviskar¹

Received: 10 August 2023 / Accepted: 13 November 2023 / Published online: 20 December 2023
© The Author(s), under exclusive licence to Springer-Verlag France SAS, part of Springer Nature 2023

Abstract

A growing trend in the utilization of compliant micro-motion stages, which offer exceptional precision and repeatability in positioning. These stages enable the creation of dual-range positioning systems, allowing for precise positioning at the nanoscale within a centimeter-scale working area when combined with conventional stages. However, such systems often come with a high price tag and require substantial physical space. This research presents an alternative solution in the form of a compact, cost-effective XY micro-motion stage with dual-range manipulation to address these limitations. The primary objective is to maintain workspace efficiency while improving positioning accuracy. This is achieved by integrating a long-range, low-resolution linear encoder with short-range, high-resolution capacitive sensors. The linear encoder determines the stage's position and provides coarse positioning data, while the capacitive sensors step in to correct any positional errors, enabling precise fine positioning. By adopting this approach, an impressive positioning precision of approximately 1.5 μm is attained within a 3 mm \times 3 mm workspace. The compliant stage is constructed using aluminum, and wire electric discharge machining is employed. This material is well-suited for this application due to its high reversible strain and compatibility with compliant systems.

Keywords Wire EDM · Micro position stage · Compliant mechanism · Sensors

1 Introduction

Because they provide a variety of advantages over conventional linear stages, such as solidity, cost savings, and improved presentation, compliant XY motion stages are viable substitutes. Such applications as micro-assembly,

semiconductor placement, fibre alignment, and AFM scanners are among the numerous sectors that employ these stages. By combining them with micro-motion applications, high levels of accuracy and repeatability in the nanoscale range have been made achievable. Compliant stages are free of backlash, friction, noise emission, and the requirement for lubrication. They do, however, have a number of drawbacks, including non-linear behaviour and a constrained working space.

The literature [1–19] has reported a number of compliant XY motion stages with motion ranges ranging from 110 to 128 mm² and positioning accuracy ranging from 10 m to a few nanometres. High accuracy and a sizable working area are frequently only possible with cost effective metrology equipment, such as ultra-high-resolution sensors and actuators with enormous range capabilities. In this study, the idea of two-range manipulation is applied in an effort to achieve positioning accuracy of a few micrometres inside a workspace at a reasonable cost.

The use of two sets of actuators and/or sensors inside the same system is known as dual-range manipulation. The second set covers a smaller area, corrects the positioning mistake

✉ Prasanna P. Raut
rautprasanna7@ymail.com

✉ Shrishail Sollapur
shrishail.sollapur@gmail.com

A. S. Rao
asrao@vjti.org.in

Devakant D. Baviskar
baviskardevakant@gmail.com

¹ Department of Mechanical Engineering, Veermata Jijabai Technological Institute, Matunga, Mumbai, Maharashtra 400019, India

² Department of International Institute for Aerospace Engineering and Management (IIAEM), Faculty of Engineering and Technology, JAIN (Deemed-to-Be University), Bengaluru, Karnataka 560069, India

of the coarse mechanism, and offers higher precision than the first set, which allows placement in a wider workspace but with less accuracy. The cost reductions, together with the avoidance of difficult calibration requirements and stringent manufacturing and assembly tolerances, are the key benefits of dual-range manipulation.

The design and assembly of traditional dual-range micro-motion stages are made simpler by the use of two serially coupled stages. Some stages use ultra-high resolution sensors, such as laser interferometers, to achieve high absolute positioning precision across a wide range of motion. However, this strategy frequently involves high expenses and has a detrimental effect on the environment. For instance, one stage design [20] layers a piezo (PZT) actuated stage on top of a DC motor-driven stage to provide a workspace of 300 mm² with positional accuracy of 10 nm. Another step [21] produces a workspace of 500500 mm² with nanometer-scale precision and a repeatability of 50 nm by using voice coil actuators (VCAs) for fine positioning and linear motors for coarse positioning. An alignment stage described in [22] combines a 2-DOF coarse positioning stage powered by linear motors with a 6-DOF fine positioning stage powered by VCAs and magnetic bearings. Within a 300mm² area, this combination yields precision of 10 nm and 15 nm along the X and Y axes, respectively. A 3-DOF stage [23] with two linear motors and four PZT actuators has an operating range of 200 mm² with an accuracy of 13 nm. The combination of VCAs with PZT actuators in the next step [24] results in an accuracy of 20 nm across a 30 mm² working area. Additionally, a 1-DOF stage [25] uses a VCA for fine motion and a linear motor for coarse motion to achieve positioning precision of 10 nm across a 350 mm working range. The geometrical dimensional values for the mechanism are represented in Table 1.

However, these expensive, highly accurate, and spacious stages are not appropriate for applications requiring the assembly of miniature products [26, 27]. Additionally, stacking two stages on top of one another adds to the moving mass, slowing the dynamic response. As an alternative, some stages employ capacitive sensors, which have excellent resolution and short range capabilities, enabling precise placement [28–34]. This method involves relative positioning based on, yet it lowers equipment expenses while keeping the same positioning precision.

2 XY motion stage design compliant

The design reported in reference [35] and the implementation in reference [36] served as the foundation for the compliant XY motion stage that is detailed in this work. The beams' dimensions were specially designed for this stage; they were

50 mm long to maximise range of motion, 8 mm tall to maintain z axis stiffness and 0.8 mm thick to reduce input force requirements. This stage is made of aluminium, a substance recognised for its high reversible strain properties, which is consistent with the bulk of compliant stages covered in the literature. At both ends of the beams, rounded corners with a radius of 0.8 mm is given to remove the factor of stress concentration.

2.1 Dynamic analysis

Ensuring the initial natural frequency of the compliant stage is as high as possible is critical to minimize the influence of external vibrations. It is also preferable to maintain a significant ratio between the first two natural frequencies and the third natural frequency. This ensures that the stiffness along the two motion directions remains much lower than the stiffness along other directions, effectively preventing undesired motion. According to existing literature [4, 5, 10–12, 37–39], the typical range for the ratio of stiffness in compliant stages varies from 3 to 6.

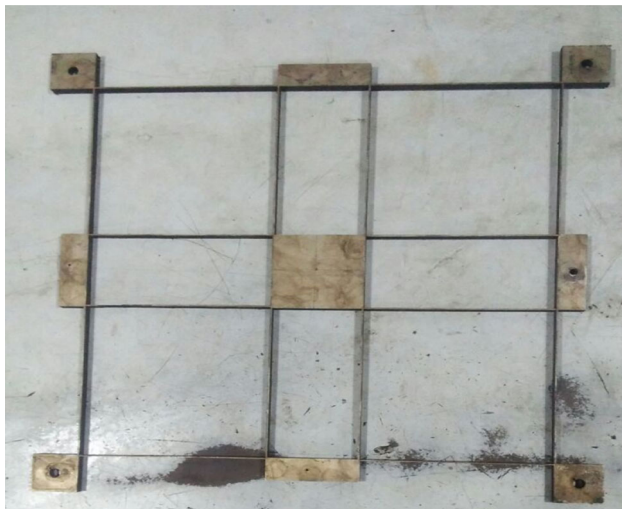
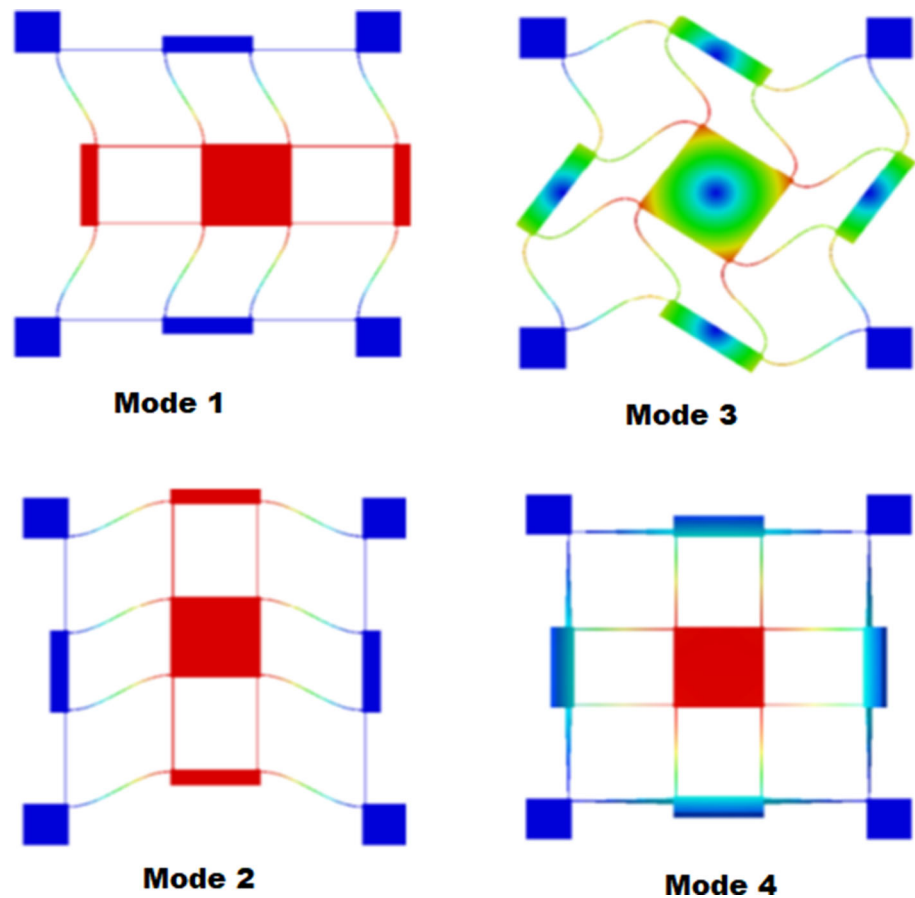
In Fig. 1, the Lanczos Eigen solver is employed for dynamic analysis in ABAQUS on the stage. The research findings indicate that the first two modes correspond to concurrent vibrations along the X and Y axes at a frequency of 57.128 Hz. In the third mode, the Z-axis undergoes rotation, with a frequency of 260.15 Hz, while the fourth mode, at a frequency of 320.03 Hz, depicts vibrations along the Z-axis. This is of utmost importance as the ratio between the first two natural frequencies and the third natural frequency exceeds 4, satisfying the essential stiffness ratio criterion.

3 Manufacturing of XY micro-motion stage

Wire electric discharge machining is used to create the majority of the compliance stages stated in the literature. Although pricey, this method provides flawless surface polishing and excellent tolerances. Alternatives including laser cutting and CNC machining were taken into consideration, but these couldn't mill 0.8 mm-thick beams. While CNC machining would result in beam bending because of the applied cutting force, laser cutting would cause the beams to melt. The stage construction was given corners with a radius of 0.8 mm in order to lessen stress concentration (Fig. 2). With an 18 mm stroke, a continuous force of 73.2 N, and a force constant of 23.16 N/A, the stage is driven by two Moticon VCA (Voice Coil Actuator). High-precision micro guides from SKF that are preloaded are used to guide the moving coils. A 12-bit Analog-to-Digital Converter (ADC) that can resolve position instructions down to 1.201 μm over 4 mm in both directions

Table 1 Basic XY motion stage geometrical dimensions

Parameters	Youngs modulus (MPa)	σ_{max} (MPa)	Density (kg/m ³)	Force (N)
Variables	71,700	508	2800	0.34

Fig. 1 FEM modal analysis with mode shapes for the mechanism**Fig. 2** XY stage designed and manufactured mechanism (37)

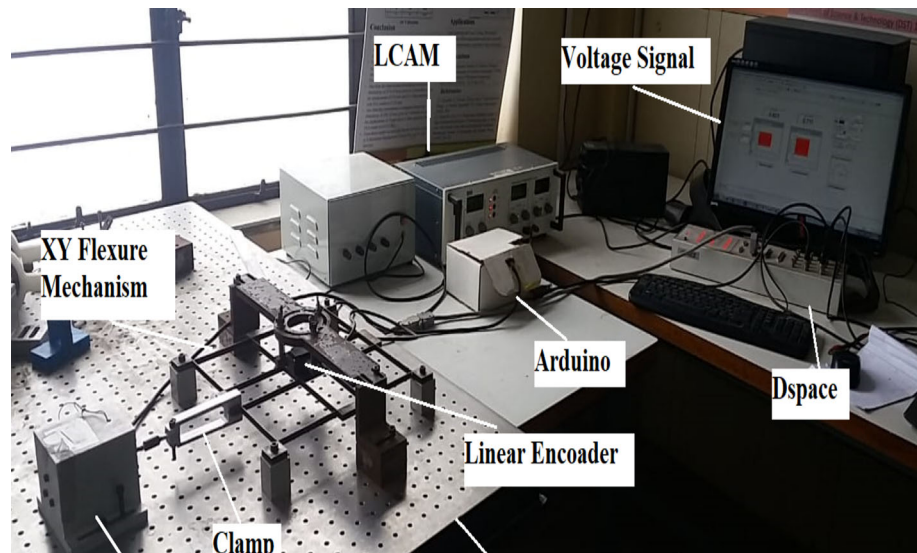
is produced by two drives operating the VCAs. The displacement of the actuators is determined by means of two Renishaw linear encoders with 115 nm precision.

3.1 Analysis of frequency response

Using testing apparatus that permits the stage to freely vibrate, the frequency response of the XY motion stage is examined as shown in Fig. 3. A 3-D accelerometer is positioned in the middle of the stage to measure the vibrations produced along the X, Y, and Z axes by an impulse. The accelerometer in use has a sensitivity of 115 mV/G. A Dual Channel Accelerometer Amplifier processes the output signal from the accelerometer, and a National Instruments data capture device with a 15 kHz sampling rate records the amplified signal.

The Fast Fourier Transform (FFT) technique is used with LabVIEW software to examine the frequency domain response of each direction of motion. Peaks may be used to

Fig. 3 Test setup for the experimentation with all components



identify the natural frequencies along each of the motion axes by looking at the amplitude spectrum. The acquired findings are compared to the FEA predictions after accounting for the accelerometer's mass.

Along the X, Y, and Z axes, the measured resonance frequency is determined to be 50 Hz, whereas it is 281 Hz along the other two axes. The associated errors are found to be 18% along the X, Y, and Z axes and 16% along the Z axis when compared to the FEA findings. The lack of adequate preloading of the beams during screwing by the mounts may account for the disparity in measurements.

4 XY two-series locating micro-motion stage

A complete XY motion range is shown in Fig. 4. It is made up of a platform that is positioned right in the centre of the complying stage. Displacement of output stage is measured using two small plates that are positioned on the platform as targets. The movable mass of the stage as a whole is around 1.8 kg.

4.1 Initial position control

A proportion-integral-derivative loop used to regulate the linear displacement of the VCAs for input position control. The stage's output displacement is sent back by the two linear encoders. Two Micro-Epsilon capacitive sensor heads (CS1) and DT controllers are employed to precisely detect the output displacement. These sensors have a obtained accuracy of 0.8 m across a series of 3 mm and a resolution of 110 nm. Two L12-P micro linear actuators are used to move them along a guide rail while they are placed on a carrier. These actuators feature a 14 mm stroke and 0.3 mm repeatability.

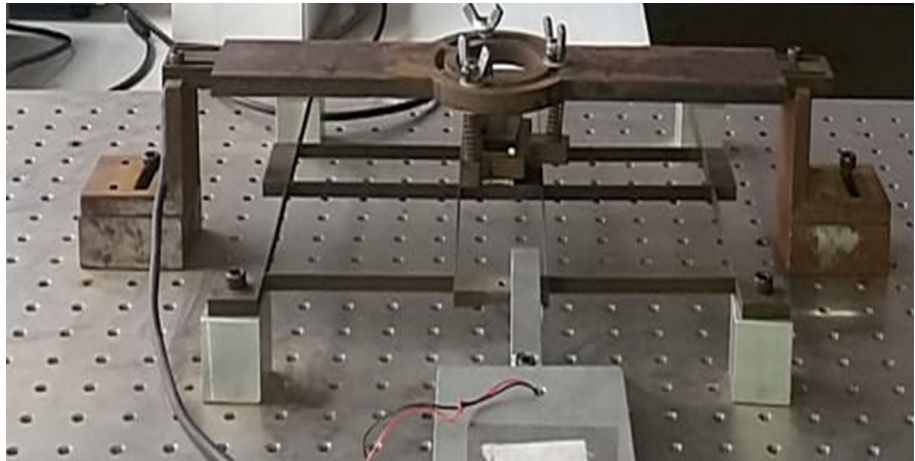
LABVIEW 2014 is used to control the input displacements along the X and Y axes of the XY motion stage using the analogue outputs of a Lab jack U6 Pro DAQ system.

The stage is displaced along the Y direction by a range of 0 to 4 mm during the single direction displacement test. The findings show that there is a 7 μm disparity between the input and output displacements. There is also a parasitic movement of 60 m in the transverse direction, which translates to a coupling of 3% (Fig. 11). Throughout the bi-directional loading test, the stage maintains the 3 mm input displacement along the Y direction while gradually applying a 4 mm input displacement along the X direction. The results, as shown in Fig. 12, are consistent with the FEA predictions with a maximum error of less than 5 m for the 4 mm input displacement. The largest parasitic displacement that has been observed is 60 μm . These data validate the stage's behaviour in comparison to the projected outcomes from finite element analysis (FEA), demonstrating the correctness and consistency of the stage's performance.

4.2 Two-range positioning

In the XY motion stage, a dual-range positioning method is used to resolve the coupling and positioning inaccuracy that have been noticed. To immediately monitor the stage's output displacement and correct the positioning fault, high-resolution sensors are used. With a 12 mm stroke and a repeatability of 0.3 mm, Firgelli L12-P micro linear actuators are used to move the sensors along a guiding rail while they are mounted on a carrier. Following are the processes involved in the two-range positioning technique for either direction of motion:

Fig. 4 Developed XY stage mechanism



1. As a coarse positioning step, the stage is first pushed into the required location in open-loop mode.
2. Next, the moving platform is approached by the high-resolution sensors, and the distance between them is measured. This distance serves as the starting location for the following phase.
3. An outside system is used to measure the positioning inaccuracy.
4. The stage is moved in closed-loop mode utilising the high-resolution sensors' feedback, and the detected positioning error is used to correct the location. The step of fine placement is this.

The output displacement of the stage is modified by a second PID loop using information from the high-resolution sensors. Gains are first adjusted by trial and error, and if more fine-tuning is necessary, it may be carried out at a later stage of development. The streamlined plant model is shown in Fig. 5, which also shows how the PID control loop and high-resolution sensors were integrated. This dual-range positioning strategy improves the XY motion stage's precision and control, providing more precise and dependable placement for a variety of applications.

The user's choice of the XY motion stage's integration into the larger system determines which external system will be used to measure positioning inaccuracy. To find the location of the movable platform where a calibration grid is placed, for instance, one possibility is to use a high-resolution vision system. In a previous study, the positional error was measured using a coordinate measuring machine (CMM) [36].

4.3 Selection of a sensor

It is crucial to use a high-resolution sensor, even when doing so requires making a trade-off between measurement precision and system cost. Table 2 uses information from RENISHAW®, KEYENCE Ltd., and MICRO-EPSILON

Ltd. to offer a qualitative analysis of four alternative sensor types for this specific application. The capacitive sensor stands out as the best choice among these alternatives since it strikes a balance between price and precision. As a result, the linear actuators are utilised in conjunction with the same sensors that were used to monitor the compliant stage's open-loop behaviour for the closed-loop control of precise placement. Figure 3 shows the layout of the XY motion stage with dual-range arrangement.

5 Experimentation

Capacitive sensors may be used to evaluate the relative positioning precision by sensing the stage's location directly. The force disturbance is thought to be more severe for larger displacements because of the nonlinear stiffness of the compliant stage. Tests are conducted with input displacements of 4 mm in both directions and no deflection in either direction in order to evaluate this. In fine positioning mode, measurements from the sensors are collected during a 28-s period, and accuracy is calculated based on the maximum oscillation amplitude after the system enters steady state.

It's also important to keep in mind that the analog-to-digital converter (ADC) that the data acquisition card uses to understand position instructions only has a 12-bit resolution. 1.8 μm of incremental position resolution is the outcome. It might be possible to achieve higher positioning precision by using controllers with higher resolution.

The steady-state response for zero loading in both directions as no external applied forces on the mechanism as shown in Fig. 6. It is clear that the greatest oscillation amplitude is less than 0.8 m, which exceeds the capacitive sensors' reading accuracy. Figure 7 on the other hand shows the reaction at steady state for a $\pm 4 \mu\text{m}$ bidirectional loading. The

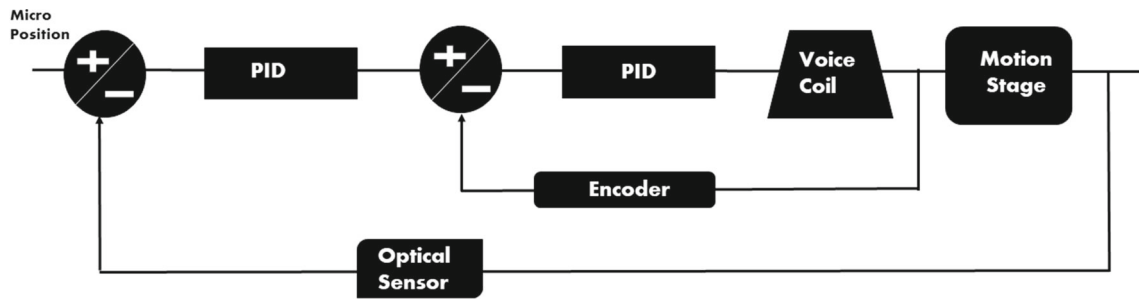


Fig. 5 Control system for accurate position for the motion stage

Table 2 Description of the sensors

Type of sensor	Accuracy	Range of sensing	Economy	Sensitivity
LVDT	–	***	***	***
Eddy current	*	–	–	***
Capacitance	***	–	*	*
Interferometer	***	**	–	*

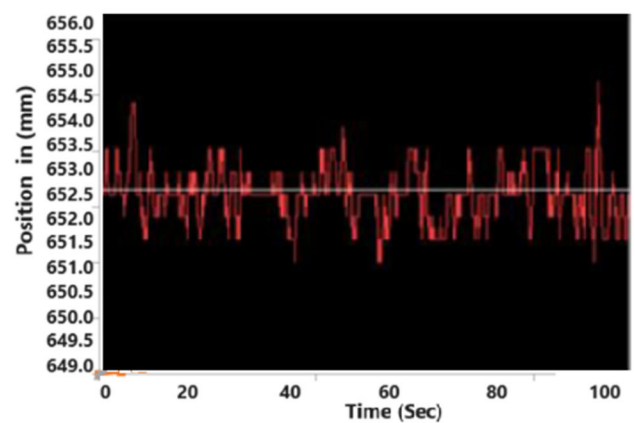
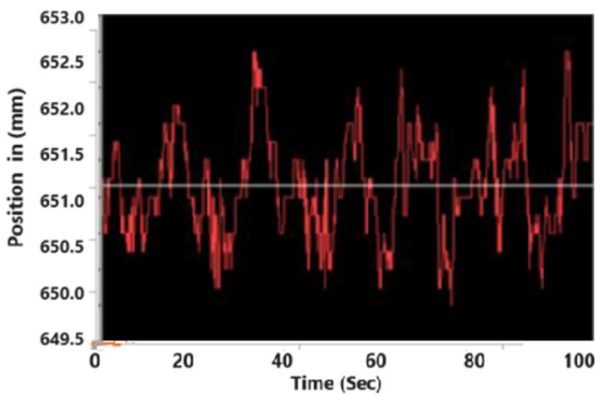
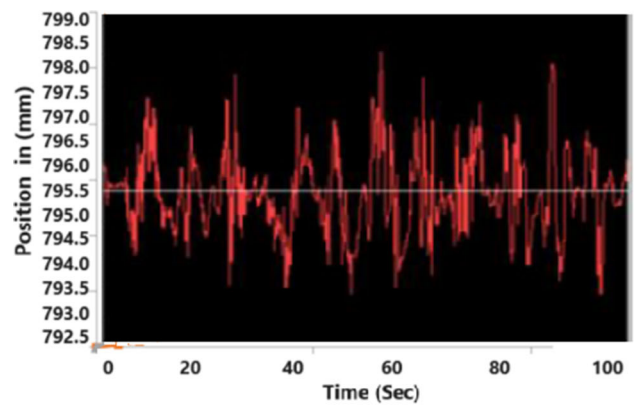
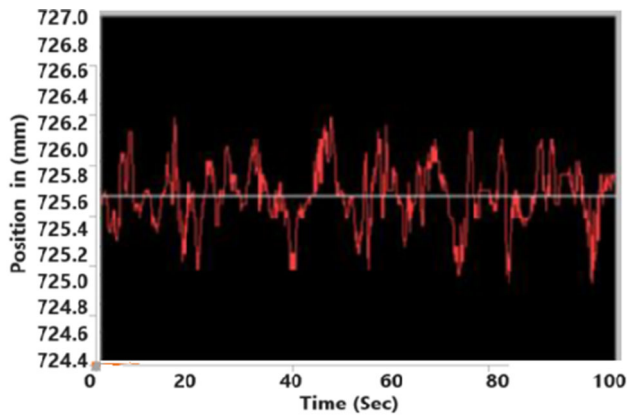


Fig. 6 X and Y axis positioning output readings from the capacitive sensors (initial 0 mm)

Fig. 7 X and Y axis positioning output readings from the capacitive sensors (final 4.0 mm)

oscillation’s amplitude grows until it reaches $\pm 4 \mu\text{m}$ demonstrating the presence of nonlinearities brought on by the compliant stage.

The design, characterization, and production of an aluminium compliant XY micro-motion stage. With a coupling ratio of 2.9%, it provides a travel range of around 4 mm in both the X and Y axes. The working area and stiffness results

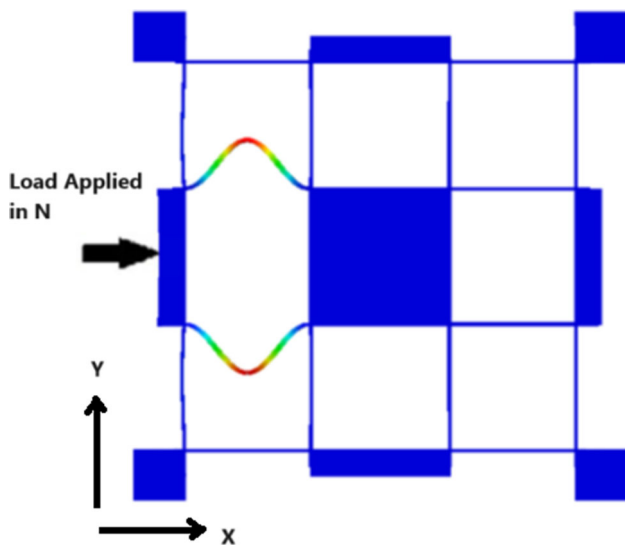


Fig. 8 Buckling point load applied in X direction

from the simulation are in good agreement with those from the finite element analysis (FEA). A maximum displacement inaccuracy of 75 μm was noted during the coarse positioning mode evaluation of the micro-motion stage.

5.1 Analysis of displacement versus force

The actuators are sized and the stage's travel range is determined using FEA analysis utilising ABAQUS. A buckling analysis and a stress/strain analysis make up the analysis.

The travel range of the stage is determined by the buckling analysis, which identifies the buckling point of the beams. Short beams may need to be subjected to much higher pressures than necessary to attain the material's yield strength before they buckle. Buckling, however, could happen before the yield strength is attained for longer or thinner beams. In this instance, buckling is observed at the inner beams Fig. 8 and the stage's difference between input and output displacement considerably widens when the stress at the centre abruptly increases. The buckling point is predicted to occur at a displacement input of about 4.257 mm, or a force input of 363.123 N, in accordance with Fig. 9.

The input displacement is gradually delivered on one side of the stage until the material's yield strength is attained before continuing with the stress/strain analysis. Throughout this evaluation, the output displacement, maximum stress, and response force are noted. In this specific instance, the reaction force of 210.011 N and the yield strength of 514 MPa are attained with an input displacement of 3.4025 mm. Thus, the stage's travel range is primarily constrained by the yield strength of the aluminium.

The final design limits the travel range in the x and y axes to 3 mm in order to guarantee a long fatigue life and reduce

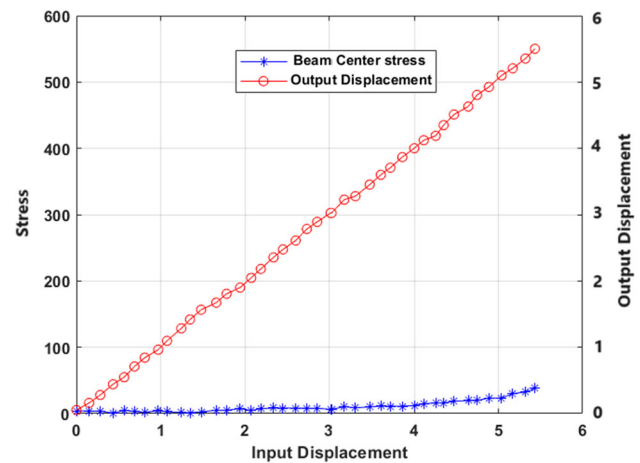


Fig. 9 Response of large displacement for the stress versus displacement

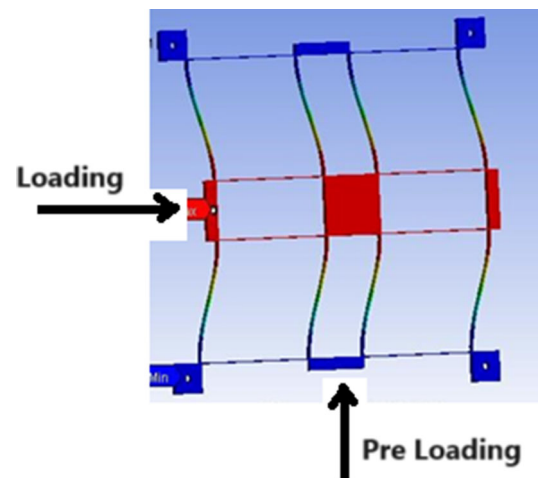


Fig. 10 X Y stage direction deformation for the motion stage

the needed force input. The input force associated with this restriction is approximately 70 N.

The axial deformation of the inner parallelogram beams is taken into account as well as a comparison of the output displacement to the input displacement. This distortion causes a little discrepancy between the output and input displacements. According to the data, the discrepancy between input and output displacements can be as much as 7 μm for input displacements between 0 and 4 mm.

5.2 Coupling analysis

For a compliant stage, minimising cross-coupling between the axes of motion is preferred. A computation is done to determine the parasitic displacement in the Y direction when a load is applied in the X direction in order to explore this. In the beginning, as represented in Fig. 10, a input displacement of 3 mm is applied along the Y direction. According to the

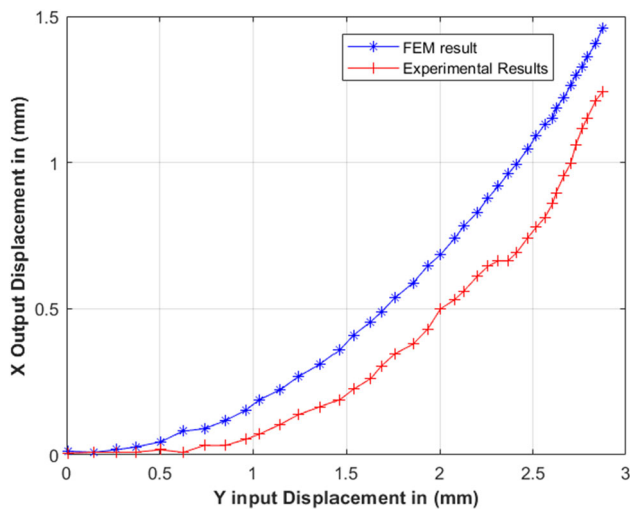


Fig. 11 One direction estimation of parasitic displacement for XY loading

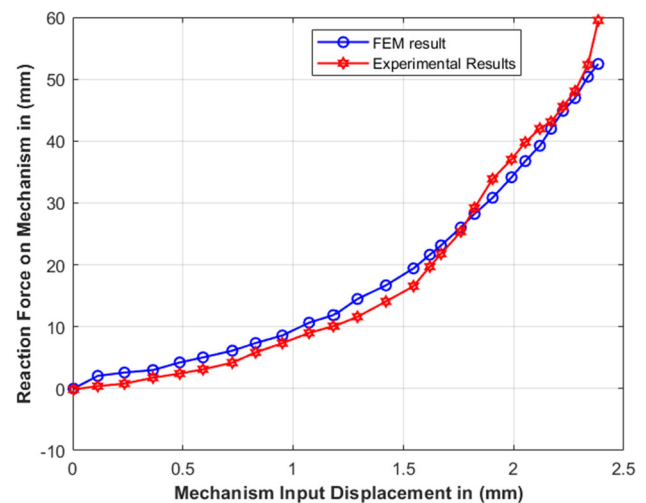


Fig. 13 One direction stiffness for the mechanism

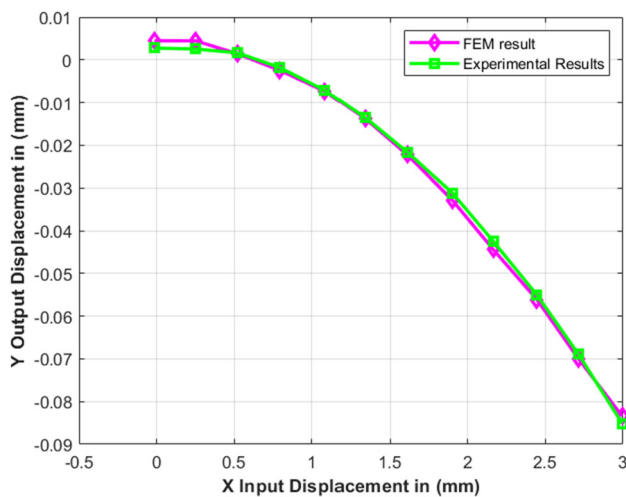


Fig. 12 Error for the XY displacement

calculations, a coupling of 5% corresponds to a maximum parasitic displacement of 75 μm (Fig. 11). Then, a 4 mm input displacement along the X direction is progressively applied. According to the findings, the greatest Y-direction displacement error is 71 μm (Fig. 12).

5.3 Force–displacement test

The relationship between input displacement and the corresponding response force was investigated in this study. While the X-axis remained fixed, the input displacement was varied along the Y-axis within the range of 0 to 4 mm. To measure the positions of the Variable Compliance Actuator (VCA), linear encoders were employed since the servo motors incorporated current sensors [40–55]. The force was subsequently determined using the VCA's force constant, and the results,

depicted in Fig. 13, reveal that the primary source of initial force inaccuracies can be attributed to internal friction in the bearings, which can be considered negligible [56–61]. When compared to the Finite Element Analysis (FEA) results, the largest force discrepancy, occurring at a 3 mm displacement, amounts to 14%. When trying to find answers to the numerous issues that are encountered in the manufacturing sector, there are a wide variety of approaches and methods that can be tried [62–70]. In the beginning, the experimental method was utilized to solve a broad variety of issues that were connected to the manufacturing sector [71–85]. As a result of developments in technology, the experimental procedures can now be evaluated, and the outcomes of those tests can be anticipated, prior to the methodologies actually being put into exercise [86–100]. The characterization strategies and procedures that are utilized by a variety of specialists in the course of the component manufacture are essential to making a significant contribution to the fields of materials and manufacturing [101–111].

6 Conclusions

A system of dual-range manipulation has been developed, utilizing capacitive sensors to enhance positioning accuracy significantly. In the most challenging scenarios, relative location accuracy has been improved to less than $\pm 4 \mu\text{m}$. The implementation of sensors with even higher resolution and advanced motor controllers is expected to further reduce this level of inaccuracy. These findings underscore the substantial potential of dual-range positioning for creating small, cost-effective, and exceptionally precise micro-motion systems. Incorporating this stage into a hybrid system for assembling

miniature products will further expand its range of applications.

Data availability Not applicable.

Declarations

Conflict of interest The authors declare that they have no conflict of interest.

References

- Wang, F., Liang, C., Tian, Y., Zhao, X., Zhang, D.: A flexure-based kinematically decoupled micropositioning stage with a centimeter range dedicated to micro/nano manufacturing. *IEEE/ASME Trans. Mechatron.* **PP**, 1–1 (2015)
- Jie, D., Sun, L., Liu, Y., Zhu, Y., Cai, H.: Design and simulation of a macro-micro dual-drive high acceleration precision XY-stage for IC bonding technology. In: *Proceeding of the 6th International Conference on Electronic Packaging Technology*, pp. 161–165 (2005)
- Tian, Y., Shirinzadeh, B., Zhang, D.: Design and dynamics of a 3-DOF flexure-based parallel mechanism for micro/nano manipulation. *Microelectron. Eng.* **87**, 230–241 (2010)
- Hao, G., Yu, J.: A completely kinematically decoupled XY compliant parallel manipulator through new topology structure. In: *Proceedings of the IFToMM Workshop on Fundamental Issues and Future Research Directions for Parallel Mechanisms and Manipulators* (2014)
- Xiao, S., Li, Y.: Design and analysis of a novel flexure-based XY micro-positioning stage driven by electromagnetic actuators. In: *Proceeding of the International Conference on Fluid Power and Mechatronics*, pp. 953–958 (2011)
- Li, Y., Huang, J., Tang, H.: A compliant parallel XY micromotion stage with complete kinematic decoupling. *IEEE Trans. Autom. Sci. Eng.* **9**, 538–553 (2012)
- Yu, J., Xie, Y., Li, Z., Hao, G.: Design and experimental testing of an improved large-range decoupled XY compliant parallel micromanipulator. *J. Mech. Robot.* **7**, 044503–044503 (2015)
- Hao, G., Kong, X.: A novel large-range XY compliant parallel manipulator with enhanced out-of-plane stiffness. *J. Mech. Des.* **134**, 061009–061009 (2012)
- Xu, Q.: New flexure parallel-kinematic micropositioning system with large workspace. *IEEE Trans. Robot.* **28**, 478–491 (2012)
- Hao, G., Meng, Q., Li, Y.: Design of large-range XY compliant parallel manipulators based on parasitic motion compensation. In: *Proceedings of the ASME international design engineering technical conferences & computers and information in engineering conference (IDETC/CIE)* (2013)
- Sollapur, S.B., Patil, M.S., Deshmukh, S.P.: Design and development aspects of flexure mechanism for high precision application. *AIP Conf. Proc.* **1943**(1), 020023 (2018)
- Sollapur, S.B., Pratik, W., Adarasha, H.: Design and experimental investigation of XY compliant mechanism for precision applications. *ECS Trans.* (2022). <https://doi.org/10.1149/10701.4967ecst>
- Waghmare, P.M.: A review paper on flexure. *Int. J. Sci. Adv. Res. Technol.* **3**(10), 544–550 (2017)
- Sollapur, S.B., et al.: Experimental investigation of high precision XY mechanism. *Int. J. Mech. Eng. Technol.* **9**(5), 43–50 (2018)
- Sollapur, S., Patil, M.S., Deshmukh, S.P.: Advancement and experimental investigation of voice coil actuator utilizing flexural bearing. *J. Mechatron. Autom. STM J.* **5**(2), 40–45 (2018)
- Sollapur, S.B., et al.: Design and experimental testing of XY flexure mechanism. *J. Eng. Sci. Technol.* **16**(2), 1416–1425 (2021)
- Sollapur, S.B.: Evaluation of stiffness and parametric modeling of XY flexure mechanism for precision applications. *J. Model. Simul. Mater.* **1**(1), 8–15 (2018). <https://doi.org/10.21467/jmsm.1.1.8-15>
- Bhaviskar, D., et al.: Design of XY planer mechanism using DFM for parallel-kinematic micro positioning XY stage. *Eur. Chem. Bull.* **11**(11), 222–228 (2022). <https://doi.org/10.48047/ecb/2022.11.11.25>
- Raut, P., et al.: Design and testing of flexural kinematic mechanism using large workspace. *Eur. Chem. Bull.* **11**(12), 213–221 (2022). <https://doi.org/10.48047/ecb/2022.11.12.025>
- Liu, C.-H., Jywe, W.-Y., Jeng, Y.-R., Hsu, T.-H., Li, Y.-T.: Design and control of a long-traveling nano-positioning stage. *Precis. Eng.* **34**, 497–506 (2010)
- Park, Y.: Precision motion control of a three degrees-of-freedom hybrid stage with dual actuators. *IET Control Theory Appl.* **2**, 392–401 (2008)
- Choi, Y.M., Gweon, D.G.: A high-precision dual-servo stage using Halbach linear active magnetic bearings. *IEEE/ASME Trans. Mechatron.* **16**, 925–931 (2011)
- Jing-Chung, S., Chia-Hung, W., Bor-Yu, C., Wen-Yuh, J.: Control of a long-stroke precision scanning stage. In: *Proceeding of the Mediterranean Conference of Control and Automation (MED)*, pp. 311–315 (2014).
- Jing-Chung, S., Wen-Yue, J., Qun-Zhong, L., Chia-Hung, W.: Control of a high precision positioning stage. In: *Proceeding of the 7th IEEE Conference on Industrial Electronics and Applications (ICIEA)*, pp. 931–935 (2012)
- Song, Y., Wang, J., Yang, K., Yin, W., Zhu, Y.: A dual-stage control system for high-speed, ultra-precise linear motion. *Int. J. Adv. Manuf. Technol.* **48**, 633–643 (2009)
- Kwon, S., Chung, W.K., Youm, Y.: On the coarse/fine dual-stage manipulators with robust perturbation compensator. In: *Proceeding of the IEEE International Conference on Robotics and Automation (ICRA)*, vol. 1, pp. 121–126 (2001)
- Zhang, L., Long, Z., Cai, J., Fang, J.: Design of a linear macro-micro actuation stage considering vibration isolation. *Adv. Mech. Eng.* **7**, 1–13 (2015)
- Jiwen, F., Zhili, L., Lufan, Z., Longsheng, N.: Driving process and control analysis in macro-micro dual stage. In: *Proceeding of the IEEE International Conference on Information and Automation (ICIA)*, pp. 37–42 (2013)
- Tang, H., Li, Y.: Design, analysis, and test of a novel 2-DOF nanopositioning system driven by dualmode. *IEEE Trans. Robot.* **29**, 650–662 (2013)
- Xu, Q.: Design and testing of a novel XY micropositioning stage with dual ranges and resolutions. In: *Proceeding of the IEEE International Conference on Robotics and Automation (ICRA)*, pp. 2351–2356 (2014)
- Sollapur, S., Patil, M.S., Deshmukh, S.P.: Position estimator algorithm implementation on precision applications. *Mater. Today Proc.* **24**, 333–342 (2020)
- Deore, O.B., Sollapur, S.: Design and analysis of compliant mechanism using FEA. *Development* **7**(10) (2020)
- Sollapur, S., Patil, M.S., Chaporkar, K., Mital, A., Bhojar, R., Dhole, K.: Design and development of constrain based XY flexural mechanism. In: Pawar, P., Ronge, B., Balasubramaniam, R., Vibhute, A., Apte, S. (eds.) *Techno-Societal 2018*. Springer, Cham (2020). https://doi.org/10.1007/978-3-030-16962-6_27
- Singh, G., Mehta, A., Bansal, A.: Electrochemical behaviour and biocompatibility of claddings developed using microwave route: review paper. *J. Electrochem. Sci. Eng.* **13**(1), 173–192 (2022). <https://doi.org/10.5599/jese.1604>

35. Herpe, X., Walker, R., Xianwen, K., Dunnigan, M.: Analysis and characterisation of a kinematically decoupled compliant XY stage. In: Proceeding of the 21st International Conference on Automation and Computing (ICAC), pp. 1–6 (2015)
36. Herpe, X., Walker, R., Dunnigan, M., Kong, X.: Design, fabrication and testing of a hybrid micro-motion XY stage driven by voice coil actuators. In: Proceeding of the International Conference for Students on Applied Engineering (ICSAE), pp. 153–158 (2016)
37. Lai, L.-J., Gu, G.-Y., Zhu, L.-M.: Design and control of a decoupled two degree of freedom translational parallel micro-positioning stage. *Rev. Sci. Instrum.* **83**, 045105 (2012)
38. Deshmukh, S.P.: X Y scanning mechanism a dynamic approach. *Int. J. Mech. Eng. Robot. Res.* **3**(4). ISSN 2278-0149. www.ijmerr.com (2014)
39. Choi, K.-B., Kim, D.-H.: Monolithic parallel linear compliant mechanism for two axes ultraprecision linear motion. *Rev. Sci. Instrum.* **77**, 065106 (2006)
40. Singh, G., Singh, R., Gul, J.: Machinability behavior of human implant materials: original scientific paper. *J. Electrochem. Sci. Eng.* **13**(1), 99–114 (2022). <https://doi.org/10.5599/jese.1514>
41. Mehta, A., Singh, G.: Consequences of hydroxyapatite doping using plasma spray to implant biomaterials: review paper. *J. Electrochem. Sci. Eng.* **13**(1), 5–23 (2023). <https://doi.org/10.5599/jese.1614>
42. Singh, G., Vasudev, H., Arora, H.: A short note on the processing of materials through microwave route. In: Singh, S., Prakash, C., Ramakrishna, S., Krolczyk, G. (eds.) *Advances in Materials Processing. Lecture Notes in Mechanical Engineering*. Springer, Singapore (2020). https://doi.org/10.1007/978-981-15-4748-5_10
43. Sharma, Y., Singh, K., Vasudev, H.: Experimental studies on friction stir welding of aluminium alloys. *Mater. Today Proc.* **50**(Part 5), 2387–2391 (2022). <https://doi.org/10.1016/j.matpr.2021.10.254>
44. Parkash, J., Saggi, H.S., Vasudev, H.: A short review on the performance of high velocity oxy-fuel coatings in boiler steel applications. *Mater. Today Proc.* **50**(Part 5), 1442–1446 (2022). <https://doi.org/10.1016/j.matpr.2021.09.014>
45. Sunitha, K., Vasudev, H.: A short note on the various thermal spray coating processes and effect of post-treatment on Ni-based coatings. *Mater. Today Proc.* **50**(Part 5), 1452–1457 (2022). <https://doi.org/10.1016/j.matpr.2021.09.017>
46. Ganesh, B., Majji, R., Vasudev, H., Bansal, A.: A review on the oxidation and wear behavior of the thermally sprayed high-entropy alloys. *Mater. Today Proc.* **50**(Part 5), 1447–1451 (2022). <https://doi.org/10.1016/j.matpr.2021.09.016>
47. Yedida, V.V.S., Vasudev, H.: A review on the development of thermal barrier coatings by using thermal spray techniques. *Mater. Today Proc.* **50**(Part 5), 1458–1464 (2022). <https://doi.org/10.1016/j.matpr.2021.09.018>
48. Singh, J., Vasudev, H., Singh, S.: Performance of different coating materials against high temperature oxidation in boiler tubes—a review. *Mater. Today Proc.* **26**(Part 2), 972–978 (2020). <https://doi.org/10.1016/j.matpr.2020.01.156>
49. Prashar, G., Vasudev, H.: Hot corrosion behavior of super alloys. *Mater. Today Proc.* **26**(Part 2), 1131–1135 (2020). <https://doi.org/10.1016/j.matpr.2020.02.226>
50. Singh, M., Vasudev, H., Kumar, R.: Microstructural characterization of BN thin films using RF magnetron sputtering method. *Mater. Today Proc.* **26**(Part 2), 2277–2282 (2020). <https://doi.org/10.1016/j.matpr.2020.02.493>
51. Mehta, A., Vasudev, H., Singh, S.: Recent developments in the designing of deposition of thermal barrier coatings—a review. *Mater. Today Proc.* **26**(22), 1336–1342 (2020). <https://doi.org/10.1016/j.matpr.2020.02.271>
52. Prashar, G., Vasudev, H., Bhuddhi, D.: Additive manufacturing: expanding 3D printing horizon in industry 4.0. *Int. J. Interact. Des. Manuf. (IJDeM)* (2022). <https://doi.org/10.1007/s12008-022-00956-4>
53. Singh, M., Vasudev, H., Singh, M.: Surface protection of SS-316L with boron nitride based thin films using radio frequency magnetron sputtering technique. *J. Electrochem. Sci. Eng.* **00**, 1–13 (2022). <https://doi.org/10.5599/jese.1247>
54. Yedida, V.V.S., Vasudev, H.: Mechanical and microstructural characterization of YSZ/Al₂O₃/CeO₂ plasma sprayed coatings: original scientific paper. *J. Electrochem. Sci. Eng.* **13**(1), 163–172 (2022). <https://doi.org/10.5599/jese.1431>
55. Prashar, G., Vasudev, H.: High temperature erosion behavior of plasma sprayed Al₂O₃ coating on AISI-304 stainless steel. *World J. Eng.* **18**(5), 760–766 (2021). <https://doi.org/10.1108/WJE-10-2020-0476>
56. Sunitha, K., Vasudev, H.: Microstructural and mechanical characterization of HVOF-sprayed Ni-based alloy coating. *Int. J. Surf. Eng. Interdiscip. Mater. Sci.* **10**(1), 1–9 (2022). <https://doi.org/10.4018/IJSEIMS.298705>
57. Singh, M., Vasudev, H., Kumar, R.: Corrosion and tribological behaviour of BN thin films deposited using magnetron sputtering. *Int. J. Surf. Eng. Interdiscip. Mater. Sci.* (2021). <https://doi.org/10.4018/IJSEIMS.2021070102>
58. Vasudev, H., Prashar, G., Thakur, L., Bansal, A.: Electrochemical corrosion behavior and microstructural characterization of HVOF sprayed Inconel-718 coating on gray cast iron. *J. Fail. Anal. Prev.* (2020). <https://doi.org/10.1007/s11668-020-01057-8>
59. Vasudev, H.: Wear characteristics of Ni-WC powder deposited by using a microwave route on mild steel: microwave cladding of Ni-WC. *Int. J. Surf. Eng. Interdiscip. Mater. Sci.* **8**(1), 44–54 (2020). <https://doi.org/10.4018/IJSEIMS.2020010104>
60. Prashar, G., Vasudev, H.: Structure-property correlation and high-temperature erosion performance of Inconel625-Al₂O₃ plasma-sprayed bimodal composite coatings. *Surf. Coat. Technol.* (2022). <https://doi.org/10.1016/j.surfcoat.2022.128450>
61. Prashar, G., Vasudev, H.: Structure-property correlation of plasma-sprayed Inconel625-Al₂O₃ bimodal composite coatings for high-temperature oxidation protection. *J. Therm. Spray Technol.* **31**, 2385–2408 (2022). <https://doi.org/10.1007/s11666-022-01466-1>
62. Prashar, G., Vasudev, H.: Thermal barrier coatings: recent developments challenges, and probable solutions. *Surf. Rev. Lett.* (2022). <https://doi.org/10.1142/S0218625X22400078>
63. Dutta, V., Thakur, L., Singh, B., Vasudev, H.: A study of erosion-corrosion behaviour of friction stir-processed chromium-reinforced NiAl bronze composite. *Materials* **15**(15), 5401 (2022). <https://doi.org/10.3390/ma15155401>
64. Singh, P., Vasudev, H., Bansal, A.: Effect of post heat-treatment on the microstructural, mechanical and bioactivity behavior of the microwave-assisted alumina reinforced hydroxyapatite cladding. Part E *J. Process Mech. Eng.* (2022). <https://doi.org/10.1177/09544089221116168>
65. Prashar, G., Vasudev, H., Thakur, L., Bansal, A.: Performance of thermally sprayed hydroxyapatite coatings for biomedical implants: a comprehensive review. *Surf. Rev. Lett.* **30**(01), 2241001 (2023). <https://doi.org/10.1142/S0218625X22410013>
66. Vasudev, H., Thakur, L., Singh, H., Bansal, A.: Effect of addition of Al₂O₃ on the high-temperature solid particle erosion behaviour of HVOF sprayed Inconel-718 coatings. *Mater. Today Commun.* **30**, 103017 (2022). <https://doi.org/10.1016/j.mtcomm.2021.103017>
67. Srinivasa Rao, G., Mukkamala, U., Hanumanthappa, H., Durga Prasad, C., Vasudev, H., Shanmugam, B., Kishore Kumar, KCh.: Evaluating and optimizing surface roughness using genetic algorithm and artificial neural networks during turning of AISI 52100

- steel. *Int. J. Interact. Des. Manuf. (IJIDeM)* (2023). <https://doi.org/10.1007/s12008-023-01549-5>
68. Manjunatha, C., Sreenivasa, T.N., Sanjay, P., Durga Prasad, C.: Optimization of friction stir welding parameters to enhance weld nugget hardness in AA6061-B4C composite material. *J. Inst. Eng. (India) Ser. D* (2023). <https://doi.org/10.1007/s40033-023-00562-y>
 69. Arunadevi, M., Rani, M., Sibinraj, R., Chandru, M.K., Durga Prasad, C.: Comparison of k-nearest neighbor & artificial neural network prediction in the mechanical properties of aluminum alloys. *Mater. Today Proc.* (2023). <https://doi.org/10.1016/j.matpr.2023.09.111>
 70. Sharanabasava, H., Raviprakash, M., Durga Prasad, C., Ramesh, M. R., Phanibhushana, M.V., Vasudev, H., Kumar, S.: Microstructure, mechanical and wear properties of SiC and Mo reinforced NiCr microwave cladding. In: *Advances in Materials and Processing Technologies*. Taylor and Francis (2023). <https://doi.org/10.1080/2374068X.2023.2257937>
 71. Durga Prasad, C., Kollur, S., Nusrathulla, M., SatheeshBabu, G., Hanamantraygouda, M.B., Prashanth, B.N., Nagabhushana, N.: Characterisation and wear behaviour of SiC reinforced FeNiCrMo composite coating by HVOF process. *Trans. IMF* (2023). <https://doi.org/10.1080/00202967.2023.2246259>
 72. Kattimani, M.A., Venkatesh, P.R., Kirthan, L.J., Math, M.M., Prapul Chandra, A.C., Hegde, R., Durga Prasad, C., Gupta, M., Kumar, S.: Design and optimization of fatigue life studies on induction hardened IN718 alloy for gas turbine applications. *Adv. Mater. Process. Technol.* (2023). <https://doi.org/10.1080/2374068X.2023.2256121>
 73. Kumar, A., Tavadi, R., Nagabhushana, N., VivekBhandarkar, V.N., Jagadeesha, T., Kerur, M.R., Rudresha, S., Durga Prasad, C., Rajesh Kannan, A., Mohan, D.G.: Investigation on mechanical and sliding wear behaviour of Pongamia-oil-cake/basalt fibre reinforced epoxy hybrid composites. *Arab. J. Sci. Eng.* (2023). <https://doi.org/10.1007/s13369-023-08207-8>
 74. Kattimani, M.A., Venkatesh, P.R., Masum, H., Math, M.M., Bahadurdesai, V.N., Mustafkhadri, S., Durga Prasad, C., Vasudev, H.: Design and numerical analysis of tensile deformation and fracture properties of induction hardened Inconel 718 superalloy for gas turbine applications. *Int. J. Interact. Des. Manuf. (IJIDeM)* (2023). <https://doi.org/10.1007/s12008-023-01452-z>
 75. Rajesh Kannan, A., Durga Prasad, C., Rajkumar, V., Siva Shanmugam, N., Rajkumar, V., Lee, W., Yoon, J.: Hot oxidation and corrosion behaviour of boiler steel fabricated by wire arc additive manufacturing. *Mater. Charact.* **203**, 113113 (2023). <https://doi.org/10.1016/j.matchar.2023.113113>
 76. Kulkarni, G.S., Siddeshkumar, N.G., Durga Prasad, C., Shankar, L., Suresh, R.: Drilling of GFRP with liquid silicon rubber reinforced with fine aluminium powder on hole surface quality and tool wear using DOE. *J. Bio- Tribo-Corros.* **9**, 53 (2023). <https://doi.org/10.1007/s40735-023-00771-8>
 77. Kulkarni, S.D., Manjunatha, Chandrasekhar, U., Manjunath, K.V., Durga Prasad, C., Vasudev, H.: Design and optimization of polyvinyl-nitrile rubber for tensile strength analysis. *Int. J. Interact. Des. Manuf. (IJIDeM)* (2023). <https://doi.org/10.1007/s12008-023-01405-6>
 78. Math, M.M., Rajeswara Rao, K.V.S., Prapul Chandra, A.C., Vijayakumar, M.N., Nandini, B., Durga Prasad, C., Vasudev, H.: Design and modeling using finite element analysis for the sitting posture of computer users based on ergonomic perspective. *Int. J. Interact. Des. Manuf. (IJIDeM)* (2023). <https://doi.org/10.1007/s12008-023-01383-9>
 79. MadhuSudana Reddy, G., Durga Prasad, C., Kollur, S., Lakshmananthan, A., Suresh, R., Aprameya, C.R.: Investigation of high temperature erosion behaviour of NiCrAlY/TiO₂ plasma coatings on titanium substrate. *JOM J. Miner. Metals Mater. Soc. TMS.* (2023). <https://doi.org/10.1007/s11837-023-05894-4>
 80. Nagabhushana, P., Ramprasad, S., Durga Prasad, C., Vasudev, H., Prakash, C.: Numerical investigation on heat transfer of a nano-fluid saturated vertical composite porous channel packed between two fluid layers. *Int. J. Interact. Des. Manuf. (IJIDeM)* (2023). <https://doi.org/10.1007/s12008-023-01379-5>
 81. Praveen, N., Mallik, U.S., Shivasiddaramaih, A.G., Suresh, R., Durga Prasad, C., Shivaramu, L.: Synthesis and wire EDM characteristics of Cu–Al–Mn ternary shape memory alloys using Taguchi method. *J. Inst. Eng. (India) Ser. D* (2023). <https://doi.org/10.1007/s40033-023-00501-x>
 82. Anjaneya, G., Sunil, S., Kakkeri, S., Math, M.M., Vaibhav, M.N., Solaimuthu, C., Durga Prasad, C., Vasudev, H.: Numerical simulation of microchannel heat exchanger using CFD. *Int. J. Interact. Des. Manuf. (IJIDeM)* (2023). <https://doi.org/10.1007/s12008-023-01376-8>
 83. Poojari, M., Hanumanthappa, H., Durga Prasad, C., Jathanna, H.M., Ksheerasagar, A.R., Shetty, P., Shanmugam, B.K., Vasudev, H.: Computational modelling for the manufacturing of solar-powered multifunctional agricultural robot. *Int. J. Interact. Des. Manuf. (IJIDeM)* (2023). <https://doi.org/10.1007/s12008-023-01291-y>
 84. Manjunatha, C.J., Durga Prasad, C., Hanumanthappa, H., Rajesh Kannan, A., Mohan, D.G., Shanmugam, B.K., Venkategowda, C.: Influence of microstructural characteristics on wear and corrosion behaviour of Si₃N₄ reinforced Al2219 composites. *Adv. Mater. Sci. Eng.* (2023). <https://doi.org/10.1155/2023/1120569>
 85. Sharanabasava, H., Durga Prasad, C., Ramesh, M.R.: Characterization and wear behavior of NiCrMoSi microwave cladding. *J. Mater. Eng. Perform.* (2023). <https://doi.org/10.1007/s11665-023-07998-z>
 86. Sharanabasava, H., Durga Prasad, C., Ramesh, M.R.: Effect of Mo and SiC reinforced NiCr microwave cladding on microstructure, mechanical and wear properties. *J. Inst. Eng. (India) Ser. D* (2023). <https://doi.org/10.1007/s40033-022-00445-8>
 87. Nithin, H.S., Nishchitha, K.M., Pradeep, D.G., Durga Prasad, C., Mathapati, M.: Comparative analysis of CoCrAlY coatings at high temperature oxidation behavior using different reinforcement composition profiles. *Weld. World* **67**, 585–592 (2023). <https://doi.org/10.1007/s40194-022-01405-2>
 88. Naveen, D.C., Kakur, N., Keerthi Gowda, B.S., MadhuSudana Reddy, G., Durga Prasad, C., Shanmugam, R.: Effects of polypropylene waste addition as coarse aggregate in concrete: experimental characterization and statistical analysis. *Adv. Mater. Sci. Eng.* (2022). <https://doi.org/10.1155/2022/7886722>
 89. Gowda, V., Hanumanthappa, H., Shanmugam, B.K., Durga Prasad, C., Sreenivasa, T.N., Rajendra Kumar, M.S.: High-temperature tribological studies on hot forged Al6061-TiB₂ in-situ composites. *J. Bio Tribo-Corros.* **8**, 101 (2022). <https://doi.org/10.1007/s40735-022-00699-5>
 90. Durga Prasad, C., Joladarashi, S., Ramesh, M.R., Srinath, M.S., Channabasappa, B.H.: Comparison of high temperature wear behavior of microwave assisted HVOF sprayed CoMoCrSi-WC-CrC-Ni/WC-12Co composite coatings. *SILICON* **12**, 3027–3045 (2020). <https://doi.org/10.1007/s12633-020-00398-1>
 91. Durga Prasad, C., Joladarashi, S., Ramesh, M.R., Srinath, M.S., Channabasappa, B.H.: Effect of microwave heating on microstructure and elevated temperature adhesive wear behavior of HVOF deposited CoMoCrSi-Cr₃C₂ composite coating. *Surf. Coat. Technol.* **374**, 291–304 (2019). <https://doi.org/10.1016/j.surfcoat.2019.05.056>
 92. Durga Prasad, C., Joladarashi, S., Ramesh, M.R., Srinath, M.S., Channabasappa, B.H.: Development and sliding wear behavior of Co-Mo-Cr-Si cladding through microwave heating. *SILICON* **11**, 2975–2986 (2019). <https://doi.org/10.1007/s12633-019-0084-5>

93. Madhusudana Reddy, G., Durga Prasad, C., Patil, P., Kakur, N., Ramesh, M.R.: Elevated temperature erosion performance of plasma sprayed NiCrAlY/TiO₂ coating on MDN 420 steel substrate. *Surf. Topogr. Metrol. Prop.* **10**, 025010 (2022). <https://doi.org/10.1088/2051-672X/ac6a6e>
94. Madhusudana Reddy, G., Durga Prasad, C., Shetty, G., Ramesh, M.R., Nageswara Rao, T., Patil, P.: Investigation of thermally sprayed NiCrAlY/TiO₂ and NiCrAlY/Cr₂O₃/YSZ cermet composite coatings on titanium alloys. *Eng. Res. Express* **4**, 025049 (2022). <https://doi.org/10.1088/2631-8695/ac7946>
95. Madhusudana Reddy, G., Durga Prasad, C., Shetty, G., Ramesh, M.R., Nageswara Rao, T., Patil, P.: High temperature oxidation behavior of plasma sprayed NiCrAlY/TiO₂ & NiCrAlY/Cr₂O₃/YSZ coatings on titanium alloy. *Weld. World* (2022). <https://doi.org/10.1007/s40194-022-01268-7>
96. Naik, T., Mathapathi, M., Durga Prasad, C., Nithin, H.S., Ramesh, M.R.: Effect of laser post treatment on microstructural and sliding wear behavior of HVOF sprayed NiCrC and NiCrSi coatings. *Surf. Rev. Lett.* **29**(1), 225000 (2022). <https://doi.org/10.1142/S0218625X2250007X>
97. Madhusudana Reddy, G., Durga Prasad, C., Shetty, G., Ramesh, M.R., Nageswara Rao, T., Patil, P.: High temperature oxidation studies of plasma sprayed NiCrAlY/TiO₂ & NiCrAlY/Cr₂O₃/YSZ cermet composite coatings on MDN-420 special steel alloy. *Metallogr. Microstruct. Anal.* **10**, 642–651 (2021). <https://doi.org/10.1007/s13632-021-00784-0>
98. Mathapati, M., Amate, K., Durga Prasad, C., Jayavardhana, M.L., Hemant Raju, T.: A review on fly ash utilization. *Mater. Today Proc.* **50**(Part 5), 1535–1540 (2022). <https://doi.org/10.1016/j.matpr.2021.09.106>
99. Durga Prasad, C., Joladarashi, S., Ramesh, M.R.: Comparative investigation of HVOF and flame sprayed CoMoCrSi coating. *Am. Inst. Phys.* **2247**, 050004 (2020). <https://doi.org/10.1063/5.0003883>
100. Dinesh, R., Rohan Raykar, S., Rakesh, T.L., Prajwal, M.G., Shashank Lingappa, M., Durga Prasad, C.: Feasibility study on MoCoCrSi/ WC-Co cladding developed on austenitic stainless steel using microwave hybrid heating. *J. Mines Metals Fuels* (2021). <https://doi.org/10.18311/jmmf/2021/30113>
101. Durga Prasad, C., Lingappa, S., Joladarashi, S., Ramesh, M.R., Sachin, B.: Characterization and sliding wear behavior of CoMoCrSi+Flyash composite cladding processed by microwave irradiation. *Mater. Today Proc.* **46**, 2387–2391 (2021). <https://doi.org/10.1016/j.matpr.2021.01.156>
102. Madhu, G., MrityunjayaSwamy, K.M., Kumar, D.A., Durga Prasad, C., Harish, U.: Evaluation of hot corrosion behavior of HVOF thermally sprayed Cr₃C₂-35NiCr coating on SS 304 boiler tube steel. *Am. Inst. Phys.* **2316**, 030014 (2021). <https://doi.org/10.1063/5.0038279>
103. Durga Prasad, C., Joladarashi, S., Ramesh, M.R., Srinath, M.S.: Microstructure and tribological resistance of flame sprayed CoMoCrSi/WC-CrC-Ni and CoMoCrSi/WC-12Co composite coatings remelted by microwave hybrid heating. *J. Bio Tribo-Corros.* **6**, 124 (2020). <https://doi.org/10.1007/s40735-020-00421-3>
104. Reddy, M.S., Durga Prasad, C., Patil, P., Ramesh, M.R., Rao, N.: Hot corrosion behavior of plasma sprayed NiCrAlY/TiO₂ and NiCrAlY/Cr₂O₃/YSZ cermets coatings on alloy steel. *Surf. Interfaces* **22**, 100810 (2021). <https://doi.org/10.1016/j.surfin.2020.10.0810>
105. Durga Prasad, C., Jerri, A., Ramesh, M.R.: Characterization and sliding wear behavior of iron based metallic coating deposited by HVOF process on low carbon steel substrate. *J. Bio Tribo-Corros.* **6**, 69 (2020). <https://doi.org/10.1007/s40735-020-00366-7>
106. Durga Prasad, C., Joladarashi, S., Ramesh, M.R., Srinath, M.S., Channabasappa, B.H.: Microstructure and tribological behavior of flame sprayed and microwave fused CoMoCrSi/CoMoCrSi-Cr₃C₂ coatings. *Mater. Res. Express* **6**, 026512 (2019). <https://doi.org/10.1088/2053-1591/aaebd9>
107. Girisha, K.G., Sreenivas Rao, K.V., Durga Prasad, C.: Slurry erosion resistance of martensitic stainless steel with plasma sprayed Al₂O₃-40%TiO₂ coatings. *Mater. Today Proc.* **5**, 7388–7393 (2018). <https://doi.org/10.1016/j.matpr.2017.11.409>
108. Durga Prasad, C., Joladarashi, S., Ramesh, M.R., Srinath, M.S., Channabasappa, B.H.: Influence of microwave hybrid heating on the sliding wear behaviour of HVOF sprayed CoMoCrSi coating. *Mater. Res. Express* **5**, 086519 (2018). <https://doi.org/10.1088/2053-1591/aad44e>
109. Girisha, K.G., Durga Prasad, C., Anil, K.C., Sreenivas Rao, K.V.: Dry sliding wear behaviour of Al₂O₃ coatings for AISI 410 grade stainless steel. *Appl. Mech. Mater.* **766–767**, 585–589 (2018). <https://doi.org/10.4028/www.scientific.net/AMM.766-767.585>
110. Durga Prasad, C., Joladarashi, S., Ramesh, M.R., Sarkar, A.: High temperature gradient cobalt based clad developed using microwave hybrid heating. *Am. Inst. Phys.* **1943**, 020111 (2018). <https://doi.org/10.1063/1.5029687>
111. Girisha, K.G., Rakesh, R., Durga Prasad, C., Sreenivas Rao, K.V.: Development of corrosion resistance coating for AISI 410 grade steel. *Appl. Mech. Mater.* **813–814**, 135–139 (2015). <https://doi.org/10.4028/www.scientific.net/AMM.813-814.135>

Publisher's Note Springer Nature remains neutral with regard to jurisdictional claims in published maps and institutional affiliations.

Springer Nature or its licensor (e.g. a society or other partner) holds exclusive rights to this article under a publishing agreement with the author(s) or other rightsholder(s); author self-archiving of the accepted manuscript version of this article is solely governed by the terms of such publishing agreement and applicable law.